applied sciences

MDPI

Article

Parameter Calibration of Discrete Element Model of Wine Lees Particles

Xiaoyuan Zhang [1,2], Rui Wang [3,*], Baoan Wang [1], Jie Chen [1] and Xiaoguo Wang [2]

[1] School of Intelligent Engineering, Jinzhong College of Information, Jinzhong 030800, China; zhangxiaoyuan@jzci.edu.cn (X.Z.); wangbaoan@jzci.edu.cn (B.W.); chenjie@jzci.edu.cn (J.C.)
[2] College of Agricultural Engineering, Shanxi Agricultural University, Jinzhong 030801, China; wxg315550@sxau.edu.cn
[3] College of Mechanical and Vehicle Engineering, Taiyuan University of Technology, Taiyuan 030024, China
* Correspondence: wangrui0023@link.tyut.edu.cn

Abstract: In order to investigate the contact characteristics of the mechanical parts of the brewing robot with wine lees particles, it is essential to calibrate the parameters of the discrete elemental model of wine lees particles. This paper proposes a method based on tests of the angle of repose. The simulation test is conducted to establish a regression model and combined with physical tests to find optimization. The contact model used in simulation modeling is Hertz-Mindlin with Johnson-Kendall-Roberts. Not all discrete element model parameters of wine lees particles have a significant impact on the angle of repose, so screening through Plackett-Burman Design is performed. The results indicate that the restitution coefficient between wine lees particles and restitution coefficient between wine lees particle and steel plate have a significant impact on angle of repose. Additionally, another parameter that is difficult to obtain, namely surface energy (JKR), also plays a crucial role. The optimal value interval for these three parameters is determined by the steepest ascent test, and a linear regression model for angle of repose is built through Box-Behnken Design. The optimal values obtained are as follows: restitution coefficient between wine lees particles—0.603; restitution coefficient between wine lees particle and steel plate—0.595; JKR—0.083. Finally, in order to verify the accuracy of calibrated parameters, simulation verification tests are carried out which show that there is only a relative error rate at 0.18% between simulated angle of repose and actual angle of repose, indicating that accurate calibration parameters were achieved. This study can provide reference for selecting discrete element model parameters for wine lees particles in future research endeavors.

Keywords: wine lees particle; discrete element method; calibration of parameters; angle of repose

Citation: Zhang, X.; Wang, R.; Wang, B.; Chen, J.; Wang, X. Parameter Calibration of Discrete Element Model of Wine Lees Particles. *Appl. Sci.* **2024**, *14*, 5281. https://doi.org/10.3390/app14125281

Academic Editors: Athanasia Koliadima, John Kapolos and Konstantinos Papadimitriou

Received: 2 May 2024
Revised: 16 June 2024
Accepted: 17 June 2024
Published: 18 June 2024

1. Introduction

The Chinese distilled wine (baijiu) brewing industry is rumored to rely on fermentation to produce aroma, and the aroma is produced by distillation. It is evident that the distillation process has a significant impact on the quality of liquor. Distillation of liquor is one of the most critical links in the brewing process and also one of the most challenging aspects to automate. During distillation, it is essential to achieve gentleness, looseness, uniformity, flatness, accuracy, and thinness in order to improve alcohol distillation and ensure both yield and quality of liquor [1–3]. The quality of the distillation process is influenced by factors such as dryness and wetness of grains, fluffiness degree, feeding speed, strength, etc., making it difficult to maintain stability in both quality and efficiency. These factors can affect the overall quality of liquor production which ultimately impacts its market price. Due to subtle differences in quality among liquors, prices may vary significantly—sometimes even tenfold. Baijiu enterprises are increasingly focusing on scaling up production while also automating processes through intelligent technologies instead of manual labor. The introduction of robots into liquor production has become an inevitable trend (see Figure 1 for a depiction of loading during the distillation process) [4].

(**a**) (**b**) (**c**)

Figure 1. Loading for the steaming process. (**a**) Artificial steaming. (**b**) Semi-automatic steaming. (**c**) Steamer-filling robot.

It is challenging for the brewing robot to achieve "light, loose, even, flat, accurate and thin" in the feeding process. In order to realize these six points, numerous universities and enterprises have undertaken a series of efforts. They have designed various mechanisms to manipulate the particles before feeding. However, regardless of the type of mechanism used, it is inevitable that the machine structure will come into direct contact with the lees particles. As a result, the lees particles will create a certain resistance to the robot and simultaneously impact their form upon contact with the robot. This interaction ultimately affects both the quality and output of the produced wine. In order to accurately simulate the interaction between the winemaking robot and the particles, it is necessary to model the lees particles using discrete element software and realize the simulation solution of the resistance of the manipulator through the coupling of RecurDyn and EDEM. However, the accuracy of the discrete element simulation results depends on the particle model discrete element parameters. The model parameters include material intrinsic parameters (particle size, Poisson's ratio, shear modulus, and density), contact parameters (collision recovery coefficient, coefficient of static friction, and coefficient of rolling friction), and contact model parameters (normal/tangential modulus for the Bonding model, surface energy JKR for the Johnson-Kendall-Roberts model, etc.). The material intrinsic parameters are usually fixed and can be obtained through literature review and experimental measurements, while the contact parameters and contact model parameters are difficult to obtain directly and need to be calibrated through simulation tests [5].

Currently, in the field of agricultural engineering, many scholars have conducted a lot of research on the calibration of discrete element model parameters of particles. Yunxia Wang, Fanyi Liu, and Tao Wu calibrated the discrete elemental model parameters of corn seeds, wheat, and clayey soil, respectively, based on angle of repose simulation experiments [6–8]; Xu Bing established a non-spherical particle model of buckwheat seeds using the auto-filling method and parameterized it using a discrete element model [9]. Wang Long designed a device to simultaneously determine the angle of repose and angle of accumulation of materials and calibrated the contact parameters of cotton seeds through physical and simulation tests [10]. Balevičius measured the static friction coefficient between pea and glass by sliding test [11]. Grima and Wypych calibrated the rolling friction coefficients of dry and wet particles in the collapse test [12]. Since there are fewer studies on the parameter calibration of the lees particle model, in order to simulate the actual working conditions more accurately, this paper intends to study the parameter calibration of the lees particle model.

Although extensive research has been conducted by scholars on the virtual calibration of discrete element simulation parameters, the commonly adopted "trial and error" method lacks a standardized parameter calibration approach. As a result, some scholars have proposed a parameter calibration method based on the response surface method. For example, Santos utilized the response surface method to obtain the dynamic angle of repose of dried cherries through the rotating drum test and calibrated corresponding

parameters in discrete element simulation [13]. Xia employed the Box-Behnken design for parameter calibration of coal particles [14], while Gong Xun completed wood chips parameter calibration using biological wood chips as the research subject based on the Box-Behnken test [15].

In this study, the cohesive contact model "Hertz-Mindlin with JKR" in EDEM2022 software was selected to simulate the angle of repose of sample lees particles. The experimental tests conducted included Plackett-Burman Design, Steepest Climb Test, and Box-Behnken Design. The above three experiments were designed using Design-Expert13 software. The parameters of the discrete element model were calibrated using the physical test results of the lees particles to achieve more accurate simulation results.

2. Materials and Methods

2.1. Basic Parameters of Lees Particles

The lees particles utilized in this study were obtained from a distillery, consisting mainly of the residues remaining after the brewing of sorghum, barley, and corn. A total of 500 g of lees particles was measured post-brewing, with a mass of 398 g after drying for 5 h, resulting in a moisture content of 20.4%. Sieving was conducted using screens with apertures measuring 3 mm, 4.5 mm, and 6 mm to determine the geometric size of the lees particles. The intrinsic parameters of the lees particles were determined through consultation with relevant data and EDEM material library. The basic parameters are presented in Table 1.

Table 1. Mass of particles of various sizes.

Particle Radius Distribution/%			Densities/kg·m^{-3}	Poisson's Ratio	Shear Modulus/Pa
≤3.0 mm	3.0–4.5 mm	≧4.5 mm			
27.6%	42.5%	29.9%	1053	0.4	1.1×10^7

2.2. Experimental Methods

In this paper, a combination of physical and simulation tests [16,17] is utilized to calibrate the parameters of the discrete elemental model of wine lees. Initially, physical tests were conducted to obtain the lees particle pile using the funnel test method and measure the actual angle of repose. Subsequently, simulation tests were performed using EDEM software to screen the parameters that significantly affect the angle of repose by Plackett-Burman Design. The optimal value interval of the significant parameters was then determined by the steepest climb test. Following this, a regression model between the rest angle of lees and the significance parameters was established and optimized through Box-Behnken Design response surface analysis in order to obtain a regression equation. This equation was solved with the actual resting angle as the target value to determine an optimal value for each significance parameter. Finally, simulation tests were carried out under these calibrated parameters, and comparison between simulated rest angles of lees with their actual counterparts verified accuracy in calibration. The technical route is shown in Figure 2.

2.3. Angle of Repose Physical Tests

In this study, the funnel method was employed to conduct the test. Initially, a baffle plate (100 mm long, 55 mm wide) was placed at the bottom of the funnel (33 mm small diameter, 150 mm large diameter, 140 mm high) to prevent the particles from falling. Subsequently, the funnel was filled with lees particles (500 g). The stopper was then pulled out to the right side at a speed of 5 m/s, allowing the lees to fall and naturally pile up as depicted in Figure 3. The stacking image underwent processing, and contours were extracted using MATLAB2022 software. The angle of repose was determined through linear fitting utilizing the least squares method [18]. By conducting five repeated tests, an average value for the actual angle of repose of the lees particles was calculated to be 25.79°.

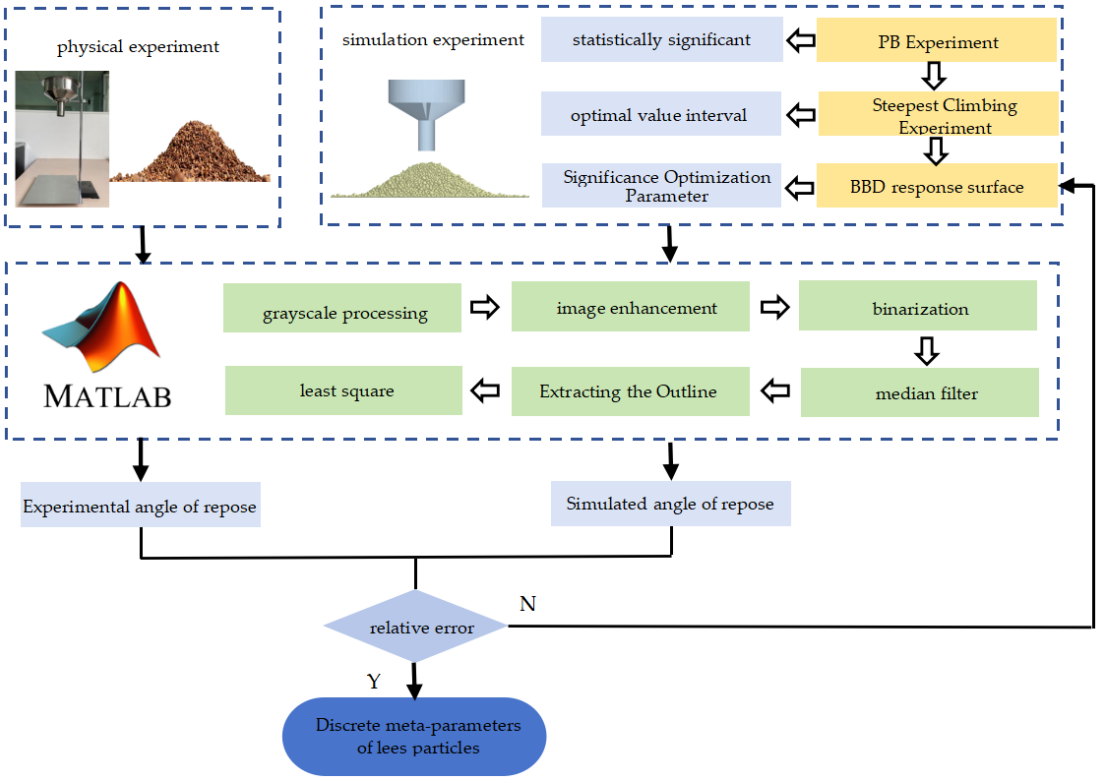

Figure 2. Technological route.

Figure 3. Particle stacking diagram.

2.4. Simulation Models

2.4.1. Contact Model

The particles in lees contain water between them, leading to an adhesion phenomenon. The classical Hertz-Mindlin contact model only considers elastic deformation and does not account for the bonding force between the particles, making it challenging to accurately simulate the behavior of lees particles. The Hertz-Mindlin with Bonding contact model uses a finite-sized "glue" to simulate particle bonding but is only suitable for simulating hard media such as rocks. On the other hand, the Hertz-Mindlin with Johnson-Kendall-Roberts (JKR) contact model is based on Hertz's theory and incorporates adhesive properties into its particle contact model. This allows for a better description of viscoelastic characteristics between particles and considers the effect of adhesive force on motion between water-containing particles. It is particularly suitable for modeling adhesion phenomena due to static electricity and moisture, such as those found in crops and soil where cohesion between lees particles is considered. Therefore, we have chosen the "Hertz-Mindlin with JKR" model as our contact model in this paper, as shown in Figure 4.

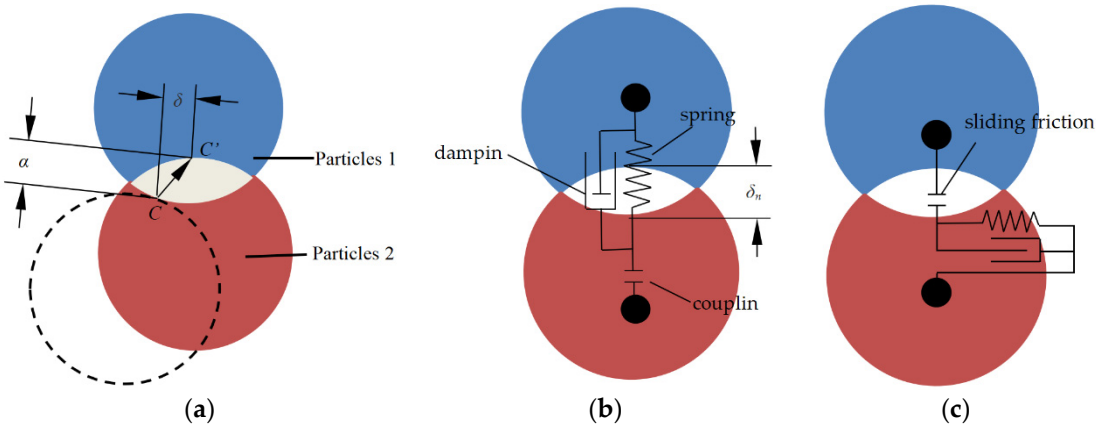

Figure 4. Softball model. (**a**) Tangential displacement. (**b**) Normal force. (**c**) Tangential force.

The normal elastic force for the Hertz-Mindlin with JKR contact model is based on the normal overlap and the surface energy, which is:

$$F_{JKR} = -4\sqrt{\pi\gamma E^*}\alpha^{\frac{3}{2}} + \frac{4E^*}{3R^*}\alpha^3 \tag{1}$$

$$\delta = \frac{\alpha^2}{R^*} - \sqrt{\frac{4\pi\gamma\alpha}{E^*}} \tag{2}$$

where F_{JKR} is the JKR normal elastic force, N; δ is the normal overlap between the two contacting particles, m; α is the tangential overlap between the two contacting particles, m; γ is the surface energy, N/m; E^* is the equivalent modulus of elasticity, Pa; and R^* is the equivalent contact radius, m. Equivalent modulus of elasticity, E^*, and equivalent contact radius, R^*, are defined as:

$$\frac{1}{E^*} = \frac{1-\nu_1^2}{E_1} + \frac{1-\nu_2^2}{E_2} \tag{3}$$

$$\frac{1}{R^*} = \frac{1}{R_1} + \frac{1}{R_2} \tag{4}$$

where E_1 and E_2 are the elastic modulus of the two contacting particles, Pa; v_1 and v_2 are the Poisson's ratios of the two contacting particles; and R_1 and R_2 are the contact radius of the two contacting particles, m. When the surface energy $\gamma = 0$, the JKR normal elastic force becomes the Hertz-Mindlin normal force:

$$F_{JKR} = F_{Hertz} = \frac{4}{3}E^*\sqrt{R^*}\delta^{\frac{3}{2}} \tag{5}$$

Even if the particles are not in direct contact, the Hertz-Mindlin with JKR contact model provides attractive cohesion, and the maximum gap between particles with non-zero cohesion is:

$$\delta_c = \frac{\alpha_c^2}{R^*} - \sqrt{\frac{4\pi\gamma\alpha_c}{E^*}} \tag{6}$$

$$\alpha_c = \left[\frac{9\pi\gamma R^{*2}}{2E^*} - \left(\frac{3}{4} - \frac{1}{\sqrt{2}}\right)\right]^{\frac{1}{3}} \tag{7}$$

where δ_c is the normal maximum gap between particles with non-zero cohesion, m; α_c is the tangential maximum gap between particles with non-zero cohesion, m.

When $\delta > \delta_c$, the inter-particle cohesion becomes zero; when the particles are not in physical contact and the spacing is less than δ_c, the cohesion reaches a maximum:

$$F_{cohesion} = -\frac{3}{2}\pi\gamma R^* \tag{8}$$

where F_{cohesion} is the cohesion force between the 2 particles, N; R^* is the equivalent contact radius, m.

The Hertz-Mindlin with JKR contact model can simulate lees particles when the separation force required to separate the 2 particles depends on the liquid surface tension and wetting angle:

$$F_{pullout} = -2\pi\gamma_s \cos(\tau)\sqrt{R_i R_j} \quad (9)$$

where F_{pullout} is the separation force required to separate the 2 particles, N; γ_s is the surface tension of the liquid, N; τ is the wetting angle, (°); and R_i, R_j are the radius of the particle, m.

2.4.2. Discrete Elemental Modeling of Particles

Due to the irregular shape of the lees particles, an amount of 500 g of lees particles with a particle size of 2~6 mm was counted and categorized into spherical, rugby ball, and flat types based on similar shapes. The geometrical dimensions of each type of particle were observed under a microscope, as shown in Figure 5a. In discrete element simulation software, spherical particles are typically used to construct discrete element models of bulk materials. However, simulating with a single spherical model cannot accurately reflect the interaction characteristics between irregular particles. To more realistically simulate the irregular characteristics of the lees particles, a discrete elemental model was established using the multi-sphere method (MSM for short) based on the geometrical dimensions of various particles given in Figure 5a [19–22]. The discrete metamodel obtained by this method closely resembles the actual appearance of lees particles. Since spherical particles would overlap and pile up, they were treated as a single body in the EDEM software, as shown in Figure 5b. The experiment utilized 1 kg of lees particles and randomly generated the mass share of each type according to the range of actual lees particle diameters.

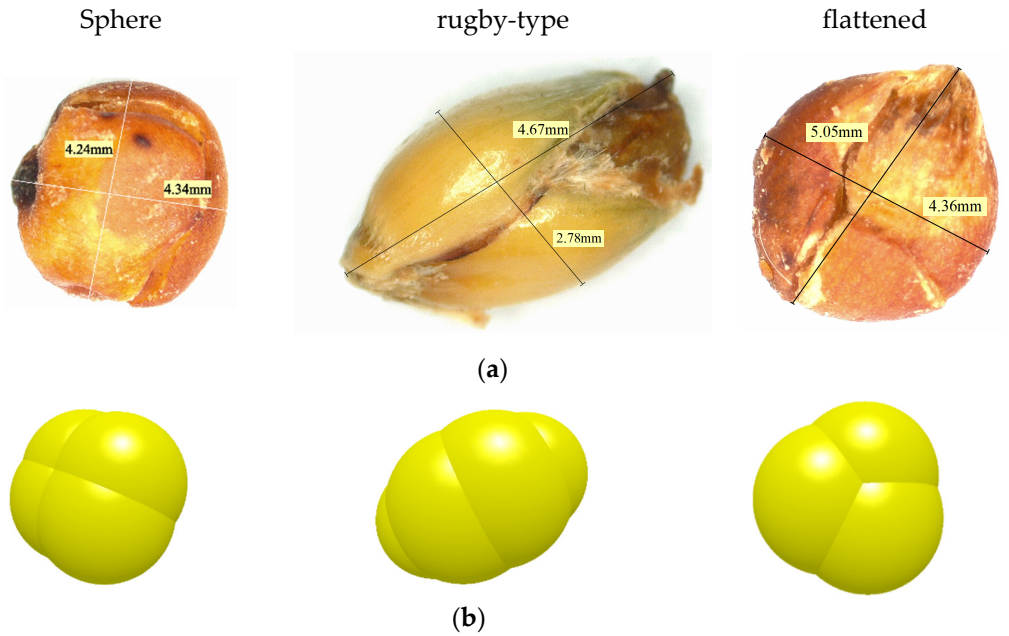

Figure 5. Wine lees particle model. (**a**) Physical model. (**b**) Discrete element model.

2.4.3. Simulation Parameter Settings

Based on the parameters of particle size and steel plate properties in discrete element simulations conducted both domestically and internationally [23–26], the range of variation for each simulation parameter in this study was determined, as shown in Table 2. During the simulation test [27], the velocity of the moving baffle plate was set to 5 m/s, consistent with physical testing conditions. Additionally, due to the influence of simulation parameters on stress wave propagation within particles, individual simulations may have different

Rayleigh time steps. Therefore, a uniform Rayleigh time step of 20% was utilized in all simulations. The grid size is defined as 5 times the size of the smallest spherical cell.

Table 2. Parameters required for EDEM simulation.

EDEM Parameters	Materials	Value	Materials	Value
Density/kg·m^{-3}	Steel	1930	Particle	1053
Poisson's ratio	Steel	0.3	Particle	0.4
Shear modulus/Pa	Steel	2×10^{11}	Particle	1.1×10^{7}
Coefficient of restitution	Particle-steel	0.4~0.8	Particle-particle	0.4~0.8
Coefficient of static friction	Particle-steel	0.5~1.0	Particle-particle	0.5~1.0
Coefficient of rolling friction	Particle-steel	0.01~0.02	Particle-particle	0.01~0.02
Surface energy/J			Particle-particle	0.05~0.1

2.4.4. Stacking Simulation Model

The parameters of the funnel were set in the simulation to match those used in the experiment. Once the particles were generated above the funnel, they fell freely and filled the entire funnel. The particles were generated using the Dynamic method at a rate of 0.25 kg/s for a duration of 4 s. Excess particles from the outside and top of the funnel were removed before running the simulation model for approximately 15 s to reach equilibrium. The baffle plate was then moved horizontally at a rate of 5 m/s, causing the particles to slowly flow out of the bottom of the funnel and eventually form a stable pile on the bottom plate. The experimental setup and simulation model are depicted in Figures 6 and 7, respectively.

Figure 6. Experimental device.

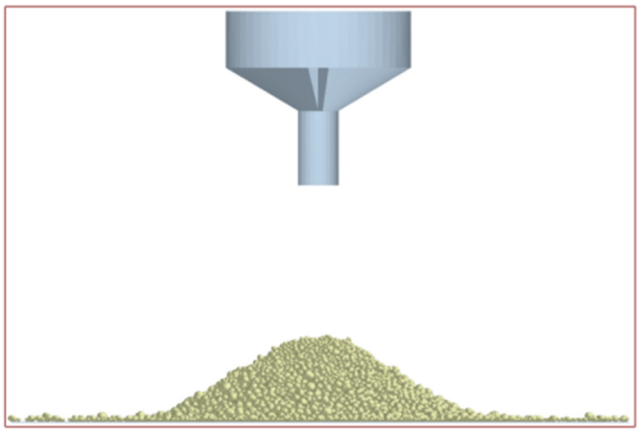

Figure 7. Simulation model.

To reduce the subjectivity and uncertainty of human measurement and to measure the angle of repose more accurately, a MATLAB image processing technique was employed to obtain the bulk angle of repose [28,29]. Firstly, the image is converted to grayscale, enhanced, and binarized (refer to Figure 8). Subsequently, the binarized image undergoes open operation and median filtering. Secondly, the boundary points of the filtered image are extracted in order to obtain the boundary curve. Finally, a linear fit is applied to the boundary curve using the least squares method to determine the slope of the fitted equation (as shown in Figure 9).

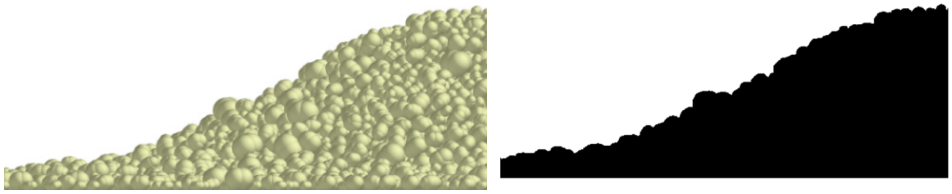

Figure 8. Image processing.

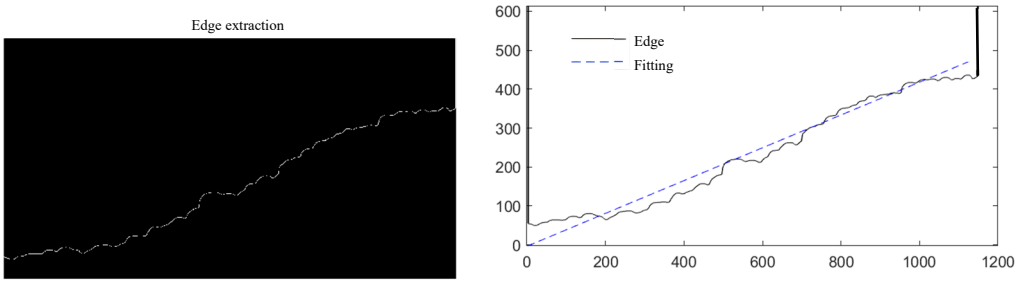

Figure 9. Edge extraction and linear fitting.

3. Results and Discussion

3.1. PB Experimental Design

3.1.1. PB Experimental Design and Results

In this study, the PB test was designed using Design-Expert's 11-factor table. Two levels of high and low were assigned to each factor, with the ratio of high level to low level set within 2.5. The study includes seven real variables, encompassing exposure parameters of the exposure model and model parameters, as well as four dummy variables for estimating errors and distinguishing the effects of different factors. The ranges of material intrinsic parameters and contact parameters are available based on references and EDEM material database. However, surface energy varies significantly with particle size and moisture content, for which no relevant reference values are provided in the literature. Therefore, pre-simulation tests are necessary to determine the range of surface energy. In summary, Table 3 presents the range of parameters for the PB experimental design.

Table 3. Parameters of PB test.

Surface Energy	Low Level	High Level
Particle-particle surface energy X_0	0.05	0.1
Particle-particle recovery coefficient X_1	0.4	0.8
Particle-particle static friction coefficient X_2	0.5	1.0
Particle-particle rolling friction coefficient X_3	0.01	0.02
Particle-steel coefficient of restitution X_4	0.4	0.8
Particle-steel static friction coefficient X_5	0.5	1.0
Particle-steel rolling friction coefficient X_6	0.01	0.02
Virtual factors V_1, V_2, V_3, V_4	−1	+1

After determining the high and low levels of the parameters, a PB test design was implemented to intercept the bulk pile from two directions spaced 180° apart. The test design and results can be found in Table 4.

Table 4. PB test design and results.

No.	X_0	X_1	V_1	X_2	X_3	V_2	X_4	X_5	V_3	X_6	V_4	Resting Angle/°
1	0.1	0.4	−1	1	0.02	1	0.8	0.5	−1	0.01	1	27.0197
2	0.05	0.4	−1	0.5	0.02	1	0.4	1	1	0.02	1	28.5799
3	0.1	0.4	1	1	0.02	−1	0.4	1	−1	0.02	−1	28.679
4	0.05	0.8	−1	1	0.01	−1	0.8	1	−1	0.02	1	13.5499
5	0.1	0.8	−1	0.5	0.02	−1	0.8	1	1	0.01	−1	14.7664
6	0.1	0.4	1	0.5	0.01	−1	0.8	0.5	1	0.02	1	25.4851
7	0.05	0.4	−1	0.5	0.01	−1	0.4	0.5	−1	0.01	−1	27.2393
8	0.05	0.8	1	1	0.02	−1	0.4	0.5	1	0.01	1	22.2007
9	0.05	0.8	1	0.5	0.02	1	0.8	0.5	−1	0.02	−1	17.5636
10	0.05	0.4	1	1	0.01	1	0.8	1	1	0.01	−1	25.9859
11	0.1	0.8	−1	1	0.01	1	0.4	0.5	1	0.02	−1	21.5922
12	0.1	0.8	1	0.5	0.01	1	0.4	1	−1	0.01	1	22.6013

3.1.2. Analysis of PB Test Results

In this study, Design-Expert was utilized to conduct an ANOVA analysis of the PB test results (refer to Table 5). The correlation coefficients of the PB test indicate that the model can account for 93.3% of the experimental variance, as evidenced by a coefficient of determination R^2 value of 0.9330, demonstrating a high degree of fit with the actual data. Additionally, R^2_{adj} = 0.8158, which is in close proximity to R^2, indicating a strong correlation; and the coefficient of variation (CV) is relatively small at 9.8%, suggesting greater precision at 7.7831. In conclusion, these findings suggest that the model exhibits high reliability and can effectively elucidate the impact of factors on response values.

Table 5. Significance analysis of PB test parameters.

Parameters	Effect	Sum of Mean Squares	Impact Rate	F	*p*	Significance Ranking
X_0	0.84	2.10	0.70	0.42	0.55	4
X_1	−8.45	214.33	70.97	42.38	0.00	1
X_2	0.47	0.65	0.22	0.13	0.74	6
X_3	0.39	0.46	0.15	0.09	0.78	7
X_4	−4.42	58.62	19.41	11.59	0.03	2
X_5	−1.16	4.01	1.33	0.79	0.42	3
X_6	−0.73	1.59	0.53	0.31	0.61	5
R^2 = 0.9330, R^2_{adj} = 0.8158, CV = 9.8%, Adeq Precision = 7.7831						

Based on the findings presented in Table 5 and Figure 10, it is evident that both the particle-particle recovery coefficient and the particle–steel plate recovery coefficient have a significant impact on the angle of repose of the lees particles. In contrast, the other contact parameters exhibit a smaller influence. Notably, the particle-particle recovery coefficient exerts a greater effect on the angle of repose compared to the particle–steel plate recovery coefficient. This can be attributed to the fact that, during the stacking process of bulk materials, only the bottom contact particles interact with the steel plate, whereas there are more interactions among lees particles.

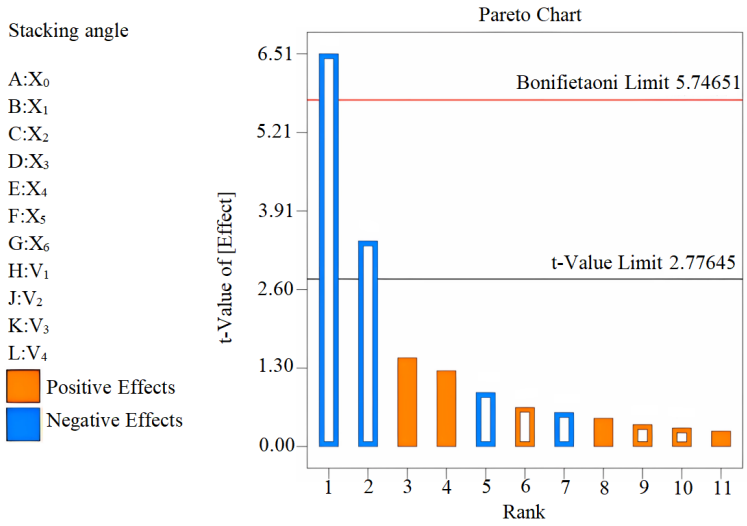

Figure 10. Pareto chart.

3.2. Steepest Climb Test

The optimal values of factors can be determined more quickly using the steepest climb test. According to the PB test results in this paper, only two significant parameters showed a gradual decrease with the selected step (indicating a negative parameter influence effect), while surface energy showed a gradual increase with the selected step (indicating a positive parameter influence effect). In this paper, Design-Expert13 software was applied to design the steepest climb test. The remaining parameters were set to an intermediate level (particle-particle static friction coefficient 0.75, particle-particle rolling friction coefficient 0.015, particle–steel plate static friction coefficient 0.75, particle–steel plate static friction coefficient 0.015) for the steepest climb test. The simulated angle of repose was then compared with the actual angle of repose of wine lees particles, and the relative error was calculated. The test program and results are shown in Table 6.

Table 6. Design parameters and results of the steepest ascent test.

No.	1	2	3	4	5
X_0	0.05	0.0625	0.075	0.0875	0.1
X_1	0.8	0.7	0.6	0.5	0.4
X_2	0.75	0.75	0.75	0.75	0.75
X_3	0.015	0.015	0.015	0.015	0.015
X_4	0.8	0.7	0.6	0.5	0.4
X_5	0.75	0.75	0.75	0.75	0.75
X_6	0.015	0.015	0.015	0.015	0.015
Resting angle/°	17.89	23.8161	26.51365	27.3669	28.4261
Relative error	30.64%	7.67%	2.79%	6.10%	10.21%

Based on the data presented in Table 6, it is evident that the particle simulation angle of repose increases as the interparticle recovery coefficient and the particle-plate recovery coefficient increase. Additionally, there is a decrease followed by an increase in the relative error between the simulated angle of repose and the actual angle of repose. The 3rd combination method exhibits the smallest relative error, suggesting that the optimal interval for the significance parameter should be close to the selected level of the 3rd set of tests. To determine this optimal value, a regression model was established using the levels of the 2nd, 3rd, and 4th groups of tests during response surface analysis testing.

3.3. Response Surface Analysis Test

3.3.1. BBD Test Design and Results

Box-Behnken response surface analysis is based on the results of the steepest climb test. Box-Behnken Design with Design-Expert Software. In this test, the non-significant parameter was chosen at the middle level, while the two significant parameters and surface energy were each taken at high, medium, and low levels, as shown in Table 7. The regression model for lees rest angle with these three parameters was established. Three center points were selected for error estimation, and the experimental design and results are presented in Table 8, comprising a total of 15 replicated tests including three center points.

Table 7. Factors and levels for Box-Behnken test.

Symbolic	Simulation Parameters	Low Level (−1)	Mid-Level (0)	High Level (1)
X_0	Particle-particle surface energy	0.0625	0.075	0.0875
X_1	Particle-particle recovery coefficient	0.5	0.6	0.7
X_4	Particle-steel recovery coefficient	0.5	0.6	0.7

Table 8. Design and results of Box-Behnken simulation test.

No.	X_0	X_1	X_4	Resting Angle/°	Relative Error
1	−1	−1	0	26.60	3.13%
2	0	1	−1	24.46	5.18%
3	0	−1	1	26.66	3.35%
4	0	0	0	25.84	0.18%
5	1	0	1	26.11	1.23%
6	0	0	0	25.84	0.18%
7	1	1	0	25.15	2.49%
8	−1	0	−1	25.99	0.76%
9	−1	1	0	24.79	3.89%
10	0	1	1	23.76	7.87%
11	1	−1	0	27.52	6.69%
12	−1	0	1	26.15	1.37%
13	0	0	0	25.84	0.18%
14	1	0	−1	26.96	4.52%
15	0	−1	−1	27.75	7.60%

3.3.2. Regression Model Analysis

Design-Expert was utilized to establish the second-order regression equation between the angle of repose and the three parameters, which is expressed as:

$$Y = 31.57 + 17.48X_1 - 0.3X_4 - 183.72X_0 + 10.1X_1 \times X_4 - 110.74X_1 \times X_0 - 200.92X_4 \times X_0 - 23.5X_1^2 + 5.17X_4^2 + 2618.92X_0^2 \quad (10)$$

The analysis of variance (ANOVA) of the quadratic regression model was performed as shown in Appendix A, Table A1, and based on the F-value and p-value, it can be obtained that the effects of the three factors on the angle of repose Y are in the order of $X_1 > X_4 > X_0 > {X_0}^2 > X_4 \times X_0 > {X_1}^2 > X_1 \times X_0 > X_1 \times X_4 > {X_4}^2$, where the particle-particle recovery coefficient is $p < 0.05$, indicating that this parameter has a significant effect on the angle of repose. This linear regression model with $p < 0.05$ shows the validity of the regression model, indicating that the relationship between the angle of repose and the resulting regression equation is significant. The coefficient of variation of the test, CV = 1.41%, indicates that the reliability of this test is good; coefficient of determination R_2 = 0.9595, Calibration coefficient of determination R_{2adj} = 0.8875, it shows that the regression equation is highly reliable; Adeq Precision = 11.9308, it shows that the accuracy of the regression model is good.

The quadratic regression model is optimized by eliminating terms that do not significantly affect the results. The optimized regression equation is as follows:

$$Y = 30.80 + 15.71X_1 + 11.97X_4 - 246.34X_0 - 200.92X_4 \times X_0 - 23.5X_1^2 + 2593.45X_0^2 \quad (11)$$

The ANOVA results of the optimized regression model are presented in Appendix A, Table A2. At this stage, the coefficient of variation (CV) is 1.22%, the coefficient of determination (R_2) is 0.9522, the corrected coefficient of determination (R_{2adj}) is 0.9164, and the precision Adeq Precision is 16.5885. Compared to the pre-optimization period, there has been a significant improvement in terms of goodness of fit, reliability, and precision in this regression equation.

The quadratic regression model was further optimized by again removing the terms with insignificant effects. The optimized regression equation is:

$$Y = 48.92 - 12.96X_1 - 3.10X_4 - 383.28X_0 + 2702.69{X_0}^2 \quad (12)$$

The analysis of variance (ANOVA) of the regression model after the secondary optimization is shown in Appendix A, Table A3, with coefficient of variation CV = 1.37%, coefficient of determination R_2 = 0.9245, corrected coefficient of determination R_{2adj} = 0.8943, and precision Adeq Precision = 17.5399. After the secondary optimization, the resultant regression equations further improved the accuracy of the model.

Applying the software Design Expert to solve the optimized regression equation with the actual rest angle of the particles as the target, we obtained optimal values for three parameters: a particle-particle recovery coefficient of 0.603, a particle-plate recovery coefficient of 0.595, and a JKR value of 0.083. By substituting these parameter values into Equation (12), we calculated a rest angle of 26.033°, which matches the experimental rest angle with a relative error of only 0.94%. This small relative error in the angle of repose demonstrates that the parameters obtained by solving for the response value are indeed valid for our purposes in this study.

Finally, Table 9 presents the discrete meta-parameters of the wine lees particles as obtained:

Table 9. DEM parameters of wine lees particles.

Parameters	Values
Particle Poisson's ratio	0.4
Particle shear modulus	1.1×10^7 Pa
Particle density	1053 kg/m^3
Particle-particle recovery factor	0.603
Particle-particle static friction coefficient	0.75
Particle-particle rolling friction coefficient	0.015
Particle-steel recovery factor	0.595
Particle-steel static friction coefficient	0.75
Particle-steel rolling friction coefficient	0.015
Surface energy	0.083

3.3.3. Analysis of Interaction Effects

Based on the results of the regression analysis using the established mathematical model, the impact of factor interactions on the response value can be objectively demonstrated in order to identify optimal process parameters through parameter interactions. The three-dimensional spatial maps, which consist of the angle of repose on particle-particle recovery coefficient, particle-plate recovery coefficient, and surface energy, provide an intuitive representation of the influence of each variable on the angle of repose. Additionally, the shapes of the contour lines reflect the strength of interaction effects, as depicted in Figure 11, Figure 12, and Figure 13, respectively.

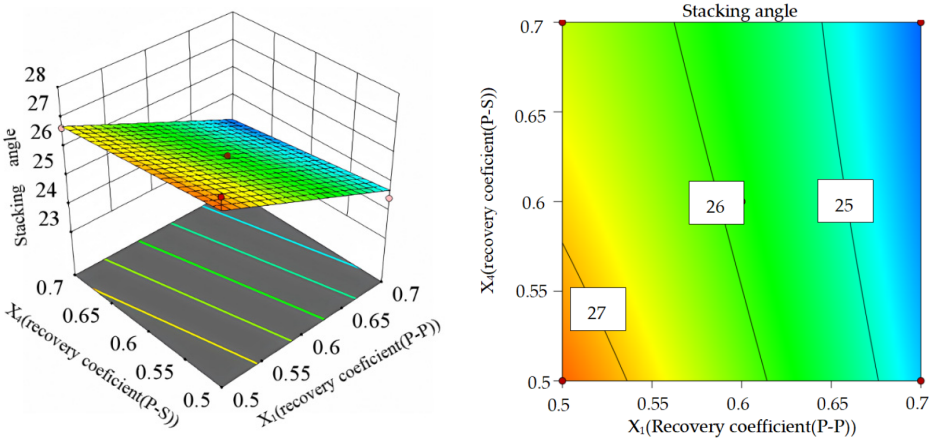

Figure 11. Three-dimensional response surface and contour plots of particle-plate recovery coefficients and particle-particle recovery coefficients for angle of repose.

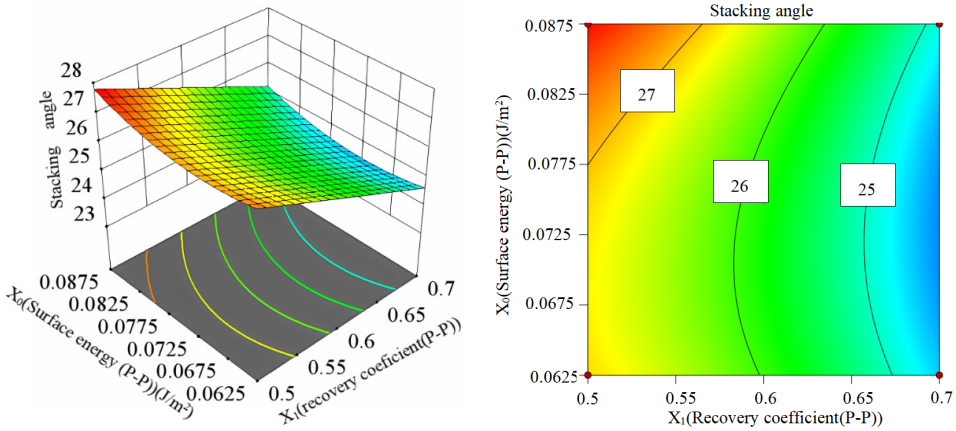

Figure 12. Three-dimensional response surface and contour plots of particle-particle recovery coefficients and surface energies against angle of repose.

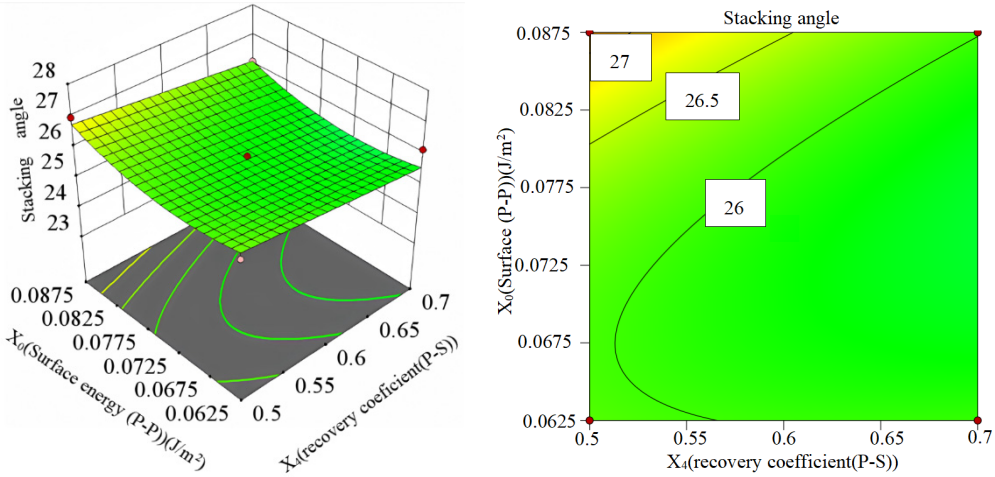

Figure 13. Three-dimensional response surface and contour plots of particle-plate recovery coefficient and surface energy against angle of repose.

3.4. Validation Experiments

To validate the accuracy of the discrete element parameters obtained, EDEM was utilized to simulate the angle of repose of lees particles by substituting the optimized discrete element parameters. The results indicate that the simulated angle of repose of lees

particles is 25.84°, which is very close to the actual angle of repose of lees particles (25.79°) with a relative error of only 0.18%. This insignificant difference proves that the optimal parameter values obtained are accurate. Figure 14 illustrates the comparison between the simulation test and physical test, showing that the heap profiles of two lees particles are highly similar.

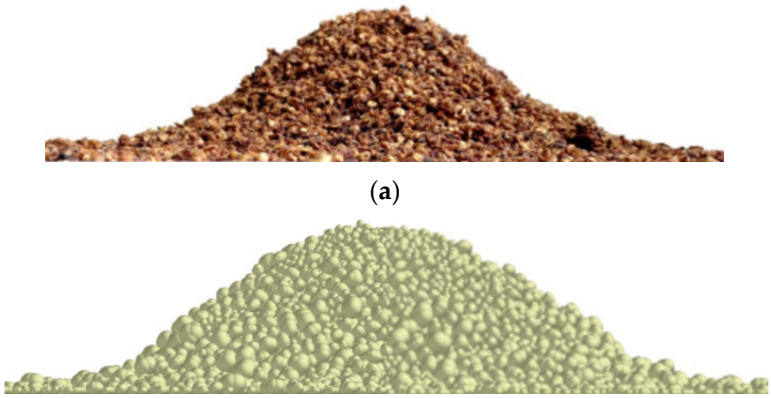

(**a**)

(**b**)

Figure 14. Comparison of simulation and physical test. (**a**) Physical test stacking image. (**b**) Simulation test stacking image.

4. Conclusions

(1) This paper utilizes EDEM discrete element simulation software to specifically analyze the lees particles in a winery. The Hertz-Mindlin with JKR contact model is selected to simulate the lees particles with a moisture content of 20.4%. Through the screening process using Plackett-Burman Design, the contact parameters and model parameters that significantly affect the angle of repose of the lees particles were identified. The results indicated that the particle-particle coefficient of recovery and the particle-plate coefficient of recovery had the most significant impact.

(2) The steepest climb test was employed to determine the optimal value ranges for significance parameters and surface energy. A regression model between the angle of repose of lees particles and these significance parameters as well as surface energy was established and optimized using the Box-Behnken Design response surface analysis test. Analysis of variance (ANOVA) revealed that, in addition to significance parameter and surface energy, the quadratic term of surface energy between particles also had a significant effect on the angle of repose of lees particles.

(3) By taking into account the actual angle of repose as an objective response value, optimization and solution techniques were applied to obtain three optimal parameter values: a particle-particle recovery coefficient of 0.603, a particle-plate recovery coefficient of 0.595, and a JKR value of 0.083.

(4) By substituting the optimal values of the discrete element parameters for the simulation test of the angle of repose of lees particles, it was found that the relative error with the experimental angle of repose is 0.18%. This result proves that the method of obtaining optimal parameter values by solving the angle of repose as the response value is effective. The comparative validation test results also demonstrate that there is no significant difference between the simulated rest angle of lees particles and the actual rest angle, thus confirming the accuracy and reliability of the calibrated discrete element model parameters for lees particles.

Author Contributions: Conceptualization, X.Z. and R.W.; software, B.W. and X.W.; validation, J.C. and X.Z.; formal analysis, R.W. and B.W.; investigation, X.Z.; writing—original draft preparation, X.Z.; writing—review and editing, X.Z., R.W. and B.W.; supervision, R.W.; project administration, X.Z. and R.W. All authors have read and agreed to the published version of the manuscript.

Funding: This research was funded by the Science and Technology Innovation Project for Higher Education Institutions in Shanxi Province (2022L659).

Institutional Review Board Statement: Not applicable.

Data Availability Statement: The data presented in this study are available upon request from the corresponding author. The data are not publicly available.

Conflicts of Interest: The authors declare no conflicts of interest.

Appendix A

Table A1. Variance analysis of regression model of BBD test.

Parameters	Sum of Mean Squares	Freedom	Mean Square	F	*p*	Significance
Models	16.08	9	1.79	13.27	0.0054	*
X_1	13.44	1	13.44	99.88	0.0002	*
X_4	0.768	1	0.768	5.71	0.062	
X_0	0.612	1	0.612	4.54	0.086	
X_1X_4	0.041	1	0.041	0.303	0.606	-
X_1X_0	0.077	1	0.077	0.569	0.485	-
X_4X_0	0.252	1	0.252	1.87	0.229	-
${X_1}^2$	0.204	1	0.204	1.51	0.273	-
${X_4}^2$	0.010	1	0.010	0.073	0.797	-
${X_0}^2$	0.618	1	0.618	4.59	0.085	
Residual	0.673	5	0.135			
Lack of Fit	0.673	3	0.224			
Pure error	0	2	0			
Cor Total	16.75	14				
	R_2 = 0.9598, R_{2adj} = 0.8875, CV = 1.41%, Adeq Precision = 11.9308					

Ps: * is significant ($p < 0.05$); - is not significant ($p > 0.1$).

Table A2. Variance analysis of optimized regression model of BBD test.

Parameters	Sum of Mean Squares	Freedom	Mean Square	F	*p*	Significance
Models	15.95	6	2.66	26.58	<0.0001	**
X_1	13.44	1	13.44	134.38	<0.0001	**
X_4	0.77	1	0.77	7.68	0.024	*
X_0	0.61	1	0.61	6.11	0.039	*
X_4X_0	0.25	1	0.25	2.52	0.151	-
${X_1}^2$	0.21	1	0.21	2.12	0.184	-
${X_0}^2$	0.61	1	0.61	6.1	0.039	*
Residual	0.80	8	0.10			
Lack of Fit	0.80	6	0.13			
Pure error	0	2	0			
Cor Total	16.75	14				
	R_2 = 0.9522, R_{2adj} = 0.9164, CV = 1.22%, Adeq Precision = 16.5885					

Ps: ** is extremely significant ($p < 0.0001$); * is significant ($p < 0.05$); - is not significant ($p > 0.1$).

Table A3. ANOVA of the regression model for secondary BBD optimization.

Parameters	Sum of Mean Squares	Freedom	Mean Square	F	*p*	Significance
Models	15.95	4	3.87	30.62	<0.0001	**
X_1	13.44	1	13.44	106.30	<0.0001	**
X_4	0.77	1	0.77	6.08	0.033	*
X_0	0.61	1	0.61	4.84	0.053	*
${X_0}^2$	0.67	1	0.67	5.26	0.045	*
Residual	1.26	10	0.13			
Lack of Fit	1.26	8	0.16			
Pure error	0	2	0			
Cor Total	16.75	14				
	R^2 = 0.9245, R^2_{adj} = 0.8943, CV = 1.37%, Adeq Precision = 17.5399					

Ps: ** is extremely significant ($p < 0.0001$); * is significant ($p < 0.05$).

References

1. Wang, X.; Jiang, Z.; Yang, J.; Qin, H.; Lei, L. Research Progress of Robot Steaming in Solid Baijiu Distillation. *Liquor. Mak.* **2024**, *51*, 32–35.
2. Li, H.L.; Huang, W.X.; Yi, B.; Yang, J.; Yang, P. Ethanol/moisture contents in fermented grains and their effects on the yield and quality of Chinese Luzhou-flavor liquor. *Adv. Mater. Res.* **2012**, *396*, 1605–1610. [CrossRef]
3. Li, H.; Huang, W.; Shen, C.; Yi, B. Optimization of the distillation process of Chinese liquor by comprehensive experimental investigation. *Food Bioprod. Process.* **2012**, *90*, 392–398. [CrossRef]
4. Tian, W. Robot Design and Experimental Research Oriented to the Steam Detection and Steaming Process. Master's Thesis, Sichuan University of Science & Engineering, Zigong, China, 2020. [CrossRef]
5. Zhang, M.; Tang, Y.; Zhang, H.; Lan, H.; Niu, H. Parameter Optimization of Spiral Fertilizer Applicator Based on Artificial Neural Network. *Sustainability* **2023**, *15*, 1744. [CrossRef]
6. Ji, J.; Jin, T.; Li, Q.; Wu, Y.; Wang, X. Construction of Maize Threshing Model by DEM Simulation. *Agriculture* **2024**, *14*, 587. [CrossRef]
7. Mou, X.; Wan, F.; Wu, J.; Luo, Q.; Xin, S.; Ma, G.; Zhou, X.; Huang, X.; Peng, L. Simulation Analysis and Multiobjective Optimization of Pulverization Process of Seed-Used Watermelon Peel Pulverizer Based on EDEM. *Agriculture* **2024**, *14*, 308. [CrossRef]
8. Li, D.; Wang, R.; Zhu, Y.; Chen, J.; Zhang, G.; Wu, C. Calibration of Simulation Parameters for Fresh Tea Leaves Based on the Discrete Element Method. *Agriculture* **2024**, *14*, 148. [CrossRef]
9. Xu, B.; Zhang, Y.; Cui, Q.; Ye, S.; Zhao, F. Construction of a discrete element model of buckwheat seeds and calibration of parameters. *INMATEH-Agric. Eng.* **2021**, *64*, 175–184. [CrossRef]
10. Wang, L.; Hu, C.; He, X.; Guo, W.; Wang, X.; Hou, S. A general modelling approach for coated cotton-seeds based on the discrete element method. *INMATEH-Agric. Eng.* **2021**, *63*, 221–230. [CrossRef]
11. Balevičius, R.; Sielamowicz, I.; Mróz, Z.; Kačianauskas, R. Investigation of wall stress and outflow rate in a flat-bottomed bin: A comparison of the DEM model results with the experimental measurements. *Powder Technol.* **2011**, *214*, 322–336. [CrossRef]
12. Grima, A.P.; Wypych, P.W. Development and validation of calibration methods for discrete element modelling. *Granul. Matter* **2011**, *13*, 127–132. [CrossRef]
13. Santos, K.G.; Campos, A.V.P.; Oliveira, O.S.; Ferreira, L.V.; Francisquetti, M.C.; Barrozo, M.A.S. Dem simulations of dynamic angle of repose of acerola residue: A parametric study using a response surface technique. *Blucher Chem. Eng. Proc.* **2015**, *1*, 11326–11333.
14. Xia, R.; Li, B.; Wang, X.; Li, T.; Yang, Z. Measurement and calibration of the discrete element parameters of wet bulk coal. *Measurement* **2019**, *142*, 84–95. [CrossRef]
15. Gong, X.; Bai, X.W.; Huang, H.; Zhang, F.; Gong, Y.; Wei, D. Dem parameters calibration of mixed biomass sawdust model with multi-response indicators. *INMATEH-Agric. Eng.* **2022**, *65*, 183–192. [CrossRef]
16. Michael, R.; Kevin, J.H. A methodical calibration procedure for discrete element models. *Powder Technol.* **2017**, *307*, 73–83. [CrossRef]
17. Coetzee, C.J. Calibration of the discrete element method. *Powder Technol.* **2017**, *310*, 104–142. [CrossRef]
18. Frączek, J.; Złobecki, A.; Zemanek, J. Assessment of angle of repose of granular plant material using computer image analysis. *J. Food Eng.* **2007**, *83*, 17–22. [CrossRef]
19. Jia, F.; Han, Y.; Liu, Y.; Cao, Y.; Shi, Y.; Yao, L.; Wang, H. Simulation prediction method of repose angle for rice particle materials. *Trans. Chin. Soc. Agric. Eng. (Trans. CSAE)* **2014**, *30*, 254–260. [CrossRef]
20. Favier, J.F.; Abbaspour-Fard, M.H.; Kremmer, M.; Raji, A.O. Shape representation of axi-symmetrical, non-spherical particles in discrete element simulation using multi-element model particles. *Eng. Comput.* **1999**, *16*, 467–480. [CrossRef]
21. Abbaspour-Fard, M.H. Theoretical validation of a multi-sphere, discrete element model suitable for biomaterials handling simulation. *Biosyst. Eng.* **2004**, *88*, 153–161. [CrossRef]
22. Kruggel-Emden, H.; Rickelt, S.; Wirtz, S.; Scherer, V. A study on the validity of the multi-sphere discrete element method. *Powder Technol.* **2008**, *188*, 153–165. [CrossRef]
23. Yu, Y.; Zhou, H.; Fu, H.; Wu, X.; Yu, J. Modeling method of corn ears based on particles agglomerate. *Trans. Csae* **2012**, *28*, 167–174. (In Chinese) [CrossRef]
24. Boac, J.M.; Casada, M.E.; Maghirang, R.G.; Harner, J.P. Material and interaction properties of selected grains and oilseeds for modeling discrete particles. *Trans. Asabe* **2010**, *53*, 1201–1216. [CrossRef]
25. Weigler, F.; Mellmann, J. Investigation of grain mass flow in a mixed flow dryer. *Particuology* **2014**, *12*, 33–39. [CrossRef]
26. Keppler, I.; Kocsis, L.; Oldal, I.; Farkas, I.; Csatar, A. Grain velocity distribution in a mixed flow dryer. *Adv. Powder Technol.* **2012**, *23*, 824–832. [CrossRef]
27. Ramírez, A.; Nielsen, J.; Ayuga, F. On the use of plate-type normal pressure cells in silos: Part 2:Validation for pressure measurements. *Comput. Electron. Agric.* **2010**, *71*, 64–70. [CrossRef]
28. Hu, J.; Xu, L.; Yu, Y.; Lu, J.; Han, D.; Chai, X.; Wu, Q.; Zhu, L. Design and Experiment of Bionic Straw-Cutting Blades Based on Locusta Migratoria Manilensis. *Agriculture* **2023**, *13*, 2231. [CrossRef]
29. Xin, M.; Jiang, Z.; Song, Y.; Cui, H.; Kong, A.; Chi, B.; Shan, R. Compression Strength and Critical Impact Speed of Typical Fertilizer Grains. *Agriculture* **2023**, *13*, 2285. [CrossRef]